PAPER

Effects of surface stability on the morphological transformation of metals and metal oxides as investigated by first-principles calculations

To cite this article: Juan Andrés *et al* 2015 *Nanotechnology* **26** 405703

View the article online for updates and enhancements.

Related content

- A 3D platform for the morphology modulation of materials: first principles calculations on the thermodynamic stability and surface structure of metal oxides: Co3O4, -Fe2O3, and In2O3
M M Ferrer, A F Gouveia, L Gracia et al.
- Identifying and rationalizing the morphological, structural, and optical properties of -Ag2MoO4 microcrystals, and the formation process of Ag nanoparticles on their surfaces: combining experimental data and first-principles calculations
Maria T Fabbro, Carla Saliby, Larissa R Rios et al.
- Modelling nanoparticles
A S Barnard

Recent citations

- Joint Theoretical and Experimental Study on the La Doping Process in In2O3: Phase Transition and Electrocatalytic Activity
S. C. S. Lemos *et al*
- In silico studies of the interaction of the colon cancer receptor and RNA aptamer adsorbed on (1 0 1) facet of TiO2 nanoparticle investigated by molecular dynamics simulation
Mohaddeseh Habibzadeh Mashatooki *et al*
- Investigation of TiO2 anatase (1 0 1), (1 0 0) and (1 1 0) facets as immobilizer for a potential anticancer RNA aptamer: a classical molecular dynamics simulation
Mohaddeseh Habibzadeh Mashatooki *et al*

IOP ebooks™

Bringing you innovative digital publishing with leading voices to create your essential collection of books in STEM research.

Start exploring the collection - download the first chapter of every title for free.

This content was downloaded from IP address 186.217.236.61 on 21/08/2019 at 17:15

IOP Publishing Nanotechnology
Nanotechnology 26 (2015) 405703 (11pp) doi:10.1088/0957-4484/26/40/405703

Effects of surface stability on the morphological transformation of metals and metal oxides as investigated by first-principles calculations

Juan Andrés[1], Lourdes Gracia[1], Amanda Fernandes Gouveia[2], Mateus Meneghetti Ferrer[2] and Elson Longo[3]

[1] Department of Analytical and Physical Chemistry, University Jaume I (UJI), Castelló E-12071, Spain
[2] INCTMN-UFSCar, Universidade Federal de São Carlos, PO Box 676, 13565-905 são Carlos, SP, Brazil
[3] INCTMN-UNESP, Universidade Estadual Paulista, PO Box 355, CEP 14801-907 Araraquara, SP, Brazil

E-mail: andres@qfa.uji.es

Received 30 June 2015, revised 13 August 2015
Accepted for publication 14 August 2015
Published 17 September 2015

Abstract

Morphology is a key property of materials. Owing to their precise structure and morphology, crystals and nanocrystals provide excellent model systems for joint experimental and theoretical investigations into surface-related properties. Faceted polyhedral crystals and nanocrystals expose well-defined crystallographic planes depending on the synthesis method, which allow for thoughtful investigations into structure–reactivity relationships under practical conditions. This feature article introduces recent work, based on the combined use of experimental findings and first-principles calculations, to provide deeper knowledge of the electronic, structural, and energetic properties controlling the morphology and the transformation mechanisms of different metals and metal oxides: Ag, anatase TiO_2, $BaZrO_3$, and α-Ag_2WO_4. According to the Wulff theorem, the equilibrium shapes of these systems are obtained from the values of their respective surface energies. These investigations are useful to gain further understanding of how to achieve morphological control of complex three-dimensional crystals by tuning the ratio of the surface energy values of the different facets. This strategy allows the prediction of possible morphologies for a crystal and/or nanocrystal by controlling the relative values of surface energies.

Keywords: morphology, Wulff theorem, surface energy

(Some figures may appear in colour only in the online journal)

1. Introduction

The ability to prepare nano- and microstructures with a well-defined morphology and excellent monodispersity at the nano- and bulk scale is an essential requirement for materials applications [1, 2]. It is generally accepted that the morphology, dimensionality, and crystal structure of the materials all play important roles in the electronic, optical, magnetic, catalytic, chemical, and other physical properties [3, 4]. Crystal morphology is governed by anisotropic surface properties, i.e., the presence of face-specific molecular arrangements, and is a critical determinant of the physical and chemical properties of crystalline materials. These molecular arrangements stem from the crystal structure and possess a symmetry that allows a group of faces, known as a family, to share identical arrangements. The anisotropic surface properties control the surface energies, growth rates, dissolution rates, wettability, cohesion, adhesion, etc. Because of the presence of surface energy anisotropy, unstable surfaces try to stabilize through the creation of low-energy surfaces; this is commonly called faceting [5]. The control of crystal morphology is a complex and difficult process, which depends

 © 2015 IOP Publishing Ltd Printed in the UK

both on the crystal internal structures and external growth conditions such as the synthesis process, the solvents used, and the process additives. In this context, Xue *et al* have developed a chemical bonding theory of single crystal growth [6, 7]. Very recently [8], these authors have reported the morphology engineering of electrode materials that can increase the performance of electrochemical energy storage devices such as Cu_2O- and MnO_2-based systems.

The relative growth rate of crystal faces, which depends on environmental conditions, evokes transformations in crystal morphology because of the appearance and/or disappearance of faces. These transformations are due to the geometric constraints imposed by the crystal structure and are associated with the relative surface energy values of each face. The observed crystal shapes are often interpreted in terms of Wulff construction [9, 10] offers a simple method to determine the equilibrium crystal shape, and different numerical implementations of this procedure are available in the literature [11–13]. Such a description is appropriate at the thermodynamic equilibrium.

This study reports results from theoretical and computational chemistry, in particular, the combination of first-principles calculations with an algorithm based on the Wulff construction, to find suitable morphological structure candidates. This perspective presents a comprehensive framework to rationalize crystal morphology and morphology evolution in crystalline materials, and summarizes our research efforts, which target the determination of the morphology in a set of materials ranging from metals to both simple and complex metal oxides: Ag, anatase TiO_2, $BaZrO_3$, and α-Ag_2WO_4. The following discussion is divided into three sections. The first section focuses on the state-of-the-art developments in this research field. The theoretical procedure and computational method are presented in section two. The third section presents the results and a process of how to create a mapping of all shape crystal possibilities to evaluate the methods to simulate suitable morphological structural candidates in order to obtain the experimental morphology of the as-synthesized samples.

1.1. State-of-the-art developments

For a crystalline material, different surfaces may have different geometric and electronic structures, and exhibit different physical and chemical properties. Accordingly, their morphology is dependent on the surface energies of the different exposed surfaces, and one may expect to tune the properties of materials by simply controlling the morphology of the crystalline materials. At the nanoscale, the ability to control the size and shape of nanocrystals (NCs) in order to tune functional properties is an important goal. The precise fabrication of NCs with specific shapes at the nanoscale level is crucial for enhancing performance in many applications [14–16]. The techniques for nanomaterial synthesis are the pillars of nanoscience and nanotechnology [17, 18]. Nanomaterial syntheses can be fine-tuned to tailor the shape of the nanomaterials, which enables the application of nanomaterials in various fields, such as catalysis [19–21] electronics [22], optics [23], and magnetism [24] etc. Hence, developing a methodology for shape-controlled NC growth is a major current research direction.

It is well established that structural changes at surfaces, including atomic relaxation and reconstruction, are a manifestation of the driving force to minimize the surface energy [25, 26]. Such shape effects result inherently from the atomic arrangement of different exposed crystal facets, and the growth mode of an NC is determined by the ratio between the growth rates of different facets [27]. Recent studies have shown that the use of capping agents is a typical and efficient strategy to control morphology and size. The functional groups on these capping agents can preferentially adsorb onto the crystal facet and modulate the kinetics of crystal growth [28–30]. Maneuvering the surface energies and growth rates of different facets determines the shape of a NC [19, 31]. Shape control of crystal growth has been reported for various types of oxide materials by modulating the reactive conditions in the liquid phase [32, 33]. In particular, surface charges and polarization have been discussed in previous reports on the synthesis of nanomaterials with some novel morphologies [34, 35]. However, the synthesis of crystals with the desired morphologies requires an understanding of the thermodynamic and kinetic mechanisms of the formation of NCs and a framework to guide the selection of environmental conditions.

Even at the nanoscale, fine control over nanoparticle (NP) morphology (surface structure) has also been shown to induce superior catalytic reactivity and selectivity [36, 37]. It is also possible to discover new and potentially useful compositions of matter on the nanoscale, because mixtures of elements that are thermodynamically unstable in the bulk may actually become stable (or metastable) as a result of quantum size-confinement effects [38, 39]. As Pauli said 'God made the bulk; surfaces were invented by the devil'.

Identifying the mechanism of the morphological transformation of both nano- and micro-crystals is crucial to gain better control of the growth of materials because the surface structure can strongly affect the crystal quality and properties. The conventional understanding of the surface atomic structure of a crystal is that facets with a higher percentage of under-coordinated atoms are usually more reactive. Modulation of morphology is a commonly employed strategy to optimize the performance of various crystalline catalysts from noble metals to semiconductors [40–42]. The synthesis of highly active facets has been considered as an important procedure to significantly promote the catalytic activity of noble metals, metal oxides, and semiconductors [43–46]. In particular, the peculiar particle morphological structures of metals and their oxides, such as cube, flower-like, octahedron, and rod, have attracted wide attention in the field of electrochemical device applications [47–49]. The basis of this strategy is that the surface atomic configuration and coordination control the reactivity and can be finely tuned by morphological control [50, 51]. The chemistry of diverse energy facets and the differences in the binding properties of the intermediates and/or products with such facets are additional determining factors in deciding the overall catalytic

activity of the materials under operating conditions. However, many questions still remain because of the lack of conclusive evidence about the mechanisms that govern crystal facet modulation at the atomic level; as such, there is considerable scope for research. In this strategy, insights from theoretical calculations and experimental evidence can be integrated with each other to develop a simple model that can be used to better understand crystal facet modulation mechanisms at the atomic level.

First-principles investigations have been recognized as effective for studying the morphology and surface properties of a wide variety of crystals and NCs [52–54]. Our group has developed a working methodology, which has been applied to the study of different morphologies in different metal oxides such as SnO_2 [55–57], $PbMoO_4$ [58], and $CaWO_4$ [59]. The relative growth rates of crystal faces, which depend on environmental conditions, cause transformations in crystal morphology because of the appearance and/or disappearance of faces. These transformations are due to the geometric constraints imposed by the crystal structure and are associated with the relative values of the surface energy of each face. In this context, Roca *et al* published some results about our simple way to use the theoretical morphology modulation in TiO_2 and α-Ag_2WO_4 [60, 61] nanocrystals in order to explain the surface energy changes observed in experimental conditions.

The main practical challenges of the present work can be summarized as follows: (i) prediction of different morphologies possible for a crystalline material, (ii) screening of relative values of surface energies to obtain desired morphologies, and (iii) target and control of crystal morphologies.

2. Theoretical procedures and computational methods

The task of predicting the morphology of crystals can be partially tackled if interest is limited to general knowledge about trends regarding bulk and surface energies (values and variations). The energetic interplay between surface energy and morphology can be identified. This section briefly presents the definition of surface energy and the Wulff construction, which are the most basic parameters and methods for predicting the equilibrium morphology of a crystal.

From the thermodynamic point of view, the equilibrium shape of a crystal is determined by the free energies of various facets, and can be calculated by the classic Wulff construction that minimizes the total surface free energy at a fixed volume [9]. The Wulff theorem provides a simple relationship between the surface energy, E_{surf}, of the (hkl) plane and its distance, rhkl, in the normal direction from the center of the crystallite. Later, the thermodynamic stability of the faceted and rounded shapes was revisited by Herring [10]. In the case when the morphology of a NC is known from microscopic observations, E_{surf} can be assessed iteratively by using the Wulff construction in the inverse fashion until the resulting shape matches the observed shape [11].

First-principles calculations were carried out using the density functional theory and implemented in the Vienna *ab initio* simulation package in order to find an ideal structure in vacuum [62, 63]. The Kohn–Sham equations were solved by means of the Perdew–Burke–Ernzerhof exchange-correlation functional [64] and the electron–ion interaction was described by the projector-augmented-wave pseudo potentials [62, 65]. The plane-wave expansion was truncated at a cut-off energy of 520 eV, and the Brillouin zones were sampled through the Monkhorst-Pack special k-points grids. The calculations were done by considering slabs with thickness of up to ~20 Å. They are sufficient to reproduce bulk-like properties at the center of the slabs, to obtain a careful description of the surfaces and to reach convergence on the corresponding energy surface values. A vacuum spacing of 15 Å is introduced in the *z*-direction so that the surfaces will not interact with each other. The positions of all atoms of the slab were allowed to relax, and the conjugated gradient energy minimization method was used to obtain relaxed systems, accomplished by requiring the forces experienced by each atom to be smaller than 0.01 eV $Å^{-1}$. E_{surf} is defined as the total energy per repeating cell of the slab (E_{slab}) minus the total energy of the perfect crystal per molecular unit (E_{bulk}) multiplied by the number of molecular units of the surface (n), divided by the surface area per repeating cell of the two sides of the slab, as following:

$$E_{surf} = \frac{E_{slab} - nE_{bulk}}{2A}.$$

The total-energy calculations are strictly valid only at zero temperature, and the entropic contribution can be taken into account by adding the computed full phonon density of states [66] or alternatively, in a simplified treatment, by inclusion of the most relevant vibration modes [67]. The crystal habits are principally determined by relative energies of the exposed planes, and entropy terms normally do not affect this ordering [68]. The entropic and pV contributions to the free energies change slightly throughout the condensed-phase species and in this type of calculation the entropic term is neglected [68–73]. Therefore, the difference between the Gibbs free energies can be approximated by the difference between the total energies from first-principles calculations [74–76].

Crystallite shape of any kind of materials can, in turn, be determined using the Wulff theorem and construction [9, 77] taking into accounts the surface energy values, implemented in the SOWOS program [13]. In this paper, this methodology was used for the morphology mapping of Ag, anatase TiO_2, $BaZrO_3$, and α-Ag_2WO_4 systems.

Several insightful review papers have reported experimental and theoretical calculations on the important aspects that govern crystal shape modulation in semiconductor and metal NPs [78–80]. In addition to the thermodynamic driving forces, kinetics also plays an important role in the determination of the morphology under real growth conditions. In such a case, the approach developed by Chernov can be applied to predict the steady-state shapes of NCs [81], and

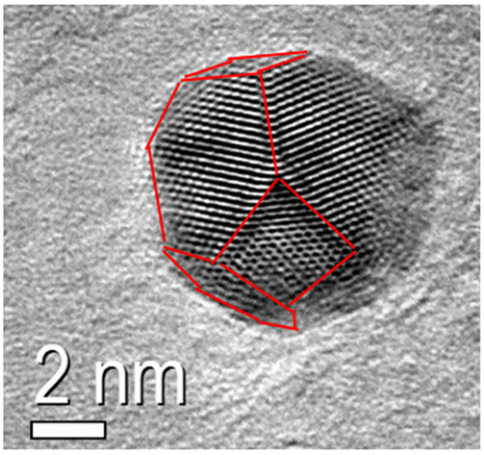

Figure 1. TEM image of Ag NC formed under electron beam irradiation.

different authors have developed strategies to calculate the velocity of facet growth [82, 83]. It was necessary, therefore, to develop a novel strategy to construct polyhedral structures and to especially address such structural issues.

3. Results and discussion

3.1. Ag

Noble metal NPs with defined structures and novel compositions are of great interest because of their potential applications in a broad range of industrially important processes [14, 84, 85]. Over the past decade, Ag NCs with a myriad of shapes (e.g., spheres, cubes, octahedrons, right bipyramids, bars, plates, rods, and wires) have been synthesized using various methods [86–88].

Recently, our research group reported the unprecedented real-time *in situ* observation of the growth process of silver metallic Ag filaments from an unstable α-Ag_2WO_4 crystal matrix when the crystal was subjected to electron irradiation from a transmission electron microscope (TEM) [89]. This is a striking result and the mechanism associated with the early events of the nucleation process of Ag has been studied in detail [90]. The crystal growth mechanism under electron beam irradiation observed in our work is completely free of additional agents, and the *in situ* TEM enables the visualization of growth of Ag NPs with planar resolution. However, an investigation of the reactions and crystal growth mechanism under electron beam irradiation can be very complicated and demands new studies [91].

An expanded image of the region around the electron driven Ag filament is illustrated in figure 1, where it is possible to identify the morphology of the Ag NC formed during the experiments. In addition, the observed NCs tend to aggregate into clusters that interact in close proximity, which implies the possible existence of an attractive force among the NCs [92, 93].

Thermodynamic calculations predict that single crystals of face-centered cubic materials such as Pt or Ag will form

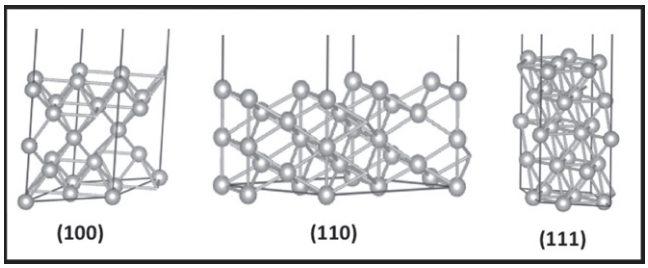

Figure 2. Surface models of (100), (110), and (111) for Ag.

truncated octahedral shapes, with the ratio of their (111) [49], and (100) type surfaces predicted through consideration of the ratio of their two respective surface energies [94]. This ratio can be significantly and controllably modified through the use of surfactants, and it has been demonstrated to have a substantial effect on catalytic selectivity [36]. Particle morphology also dictates the nearest-neighbor coordinations of the exposed surface atoms, broadly affecting the catalytic activity [95].

The morphological characterization of Ag NPs has shown strong correlations between properties such as average particle size, shape, and dispersity with observed and inherently tunable physiochemical behavior [96, 97]. In this context, Barnard *et al* [98] have presented detailed structure/property maps, showing that faceted near-spherical shapes and spheres are the predominant morphologies in Ag NPs colloidal samples at low and high temperatures. The production of well-defined NPs with reproducible size and shape distributions remains challenging [99], although different studies report clarification of stability, probability, and population in NP ensembles [100]. The (100), (110), and (111) surfaces were modeled by unreconstructed (truncated bulk) slab models by using a calculated equilibrium geometry and using a $(6 \times 6 \times 1)$ Monkhorst-Pack special k-points grid to ensure geometrical and energetic convergence for the Ag structures considered. Slab models containing 15 Ag atoms placed in 3 five-atomic layers were selected, with areas of 8.77 $Å^2$, 12.4 $Å^2$, and 7.59 $Å^2$ for the (100), (110), and (111) surfaces, respectively. Figure 2 depicts the slab representation for Ag.

An analysis of figure 3 shows that the calculated energy surface values (center of figure 3) generate a morphology very similar to that of synthesized Ag NCs, generated by matching the corresponding TEM image (see figure 1). When the difference in the stability of the facets is reduced, more than one type of facet will appear, and the resulting polyhedron should gradually appear rounder, with truncated edges and corners. When the ratio of the energy surface is varied by increasing the value of the (111) surface more than 22% because of some perturbation, the resulting morphology is a double truncated octahedron. The same morphology is obtained by decreasing the value of the (110) and (011) surfaces more than 24% with respect to the computed initial value. On the other hand, a truncated cube or a truncated octahedron can be achieved when the value of the (100) and (001) surfaces is decreased by around 42% or is increased by around 20%, respectively.

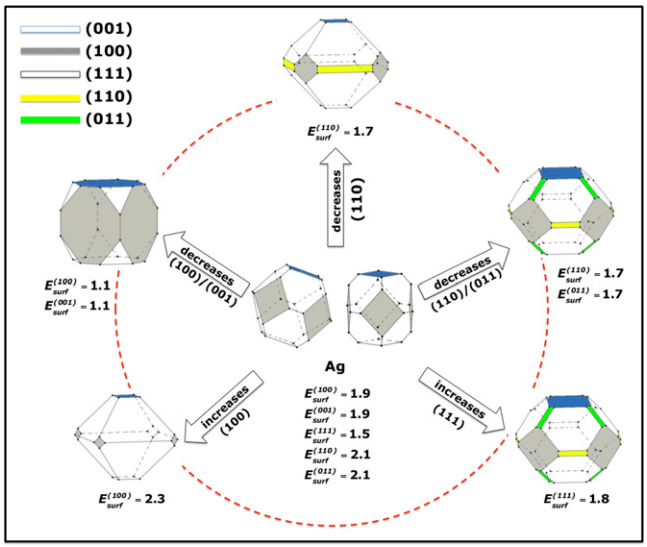

Figure 3. Crystallographic structure and map of morphologies of Ag NC with (100), (001), (111), (110), and (011) crystal planes. Surface energy is in joules per square meter. Theoretical (experimental) [102] lattice parameter, $a = 4.188$ Å (4.086 Å).

In addition, using the different morphologies displayed in figure 3, we can rationalize some experimental results reported very recently by Wang *et al* [101] such as the formation of Ag nanocubes and octahedra.

3.2. Anatase TiO_2

The morphology as well as the crystal-facet-controlled synthesis of titanium dioxide (TiO_2) has attracted interest because of its scientific and technological applications, including in photocatalysts and self-cleaning agents [103].

TiO_2 is a common multifunctional material, which has been used in a wide variety of applications in many fields, such as in ceramics, cosmetics, medicine, food, and catalysts [104]. For TiO_2, three polymorphs are stable at atmospheric pressure: the thermodynamically favored rutile phase that can be grown in bulk, and the less common anatase and brookite phases. The polymorphs have significantly different chemical reactivities with anatase and brookite typically being believed to be the most reactive. Hence, many researchers have pursued polymorph-specific syntheses of high-reactivity NCs [105]. Anatase TiO_2 was proven to be more active than the other two main TiO_2 crystal polymorphs, i.e., rutile and brookite, especially when TiO_2 is employed as a catalyst and photocatalyst [50, 106].

Under equilibrium conditions, natural and synthetic anatase TiO_2 single crystals mainly exist in an octahedral bipyramidal morphology in which a majority of the surface is normally enclosed by energetically favorable (101) facets rather than the more reactive (001) facets [107–109]. Thus, it has long been a great challenge to synthesize anatase TiO_2 with a large fraction of exposed (001) facets. However, recently, many studies have reported the synthesis of high-energy anatase surfaces [42, 110, 111].

Despite intense investigations into the preparation of specific facets, the inherent photoactivities of TiO_2 facets are still ambiguous. The (001) facet was initially expected to be the most active because of its high surface energy [42, 112–115], whereas later research suggested that the clean (010) facet with 100% five-coordinate Ti was more active in photo-oxidation and photoreduction reactions [116]. In particular, Liu *et al* reported that the photoreactivity of (010) facets of TiO_2 is higher than that of the (101) facets, while the (001) facets showed the lowest photoreactivity [116]. However, more recent research has suggested that different facets may play different roles in photoreaction [117, 118].

Based on first-principles calculations, the E_{surf} values for (101), (001), (110), and (100) facets of anatase TiO_2 were determined, using a $(4 \times 4 \times 1)$ Monkhorst-Pack special k-points grid. Slab models containing 12, 14, 24, and 16 molecular units with areas of 14.5 Å^2, 19.4 Å^2, 35.9 Å^2, and 25.4 Å^2 for the (001), (101), (100), and (110) surfaces, respectively. It is worth noting that the (001) and (101) surfaces are O-terminated, while the (100) and (110) surfaces are Ti and O-terminated. Figure 4 depicts the slab representation for anatase TiO_2. Each surface has been modeled using stoichiometric systems [119].

The E_{surf} values and the Wulff construction of the ideal structure for anatase TiO_2 in vacuum are shown in figure 5. It is possible to determine which structure should be present in anatase TiO_2 by calculating the mathematical relationships with the E_{surf} values if a few facets are more stable than others. The Wulff constructions of those structures are also shown in figure 5.

Figure 5 can be used as a tool to verify the relative value of E_{surf} that is necessary to obtain a particular morphology. Many research groups have studied anatase TiO_2 with various shapes, such as single particle, nanosheet, cube, film, and flowerlike shapes [112–114].

Theoretical results reported by Barnard *et al* [121] point out the effect of water on the morphology of anatase and rutile TiO_2. For anatase TiO_2, the presence of water resulted in a variation in the size of the (001) facets. In another paper, Barnard and Curtiss [107] show the influence of acidic and alkaline conditions on the morphology of TiO_2. The morphology shows a high occurrence of (100)/(010) facets that predominantly occur in hydrogen-poor and oxygenated conditions. We obtained the surface energies of these shape-decreasing (100)/(010) facets.

Some experimental results reported recently by Pan *et al* show an elongated, truncated tetragonal bipyramid anatase with highly exposed (010) facets that was also synthesized by tuning the Ti/F ratio [116]. This morphology was obtained by decreasing the (100)/(010) surface energy of the initial Wulff construction on the map.

The cube shape is obtained by decreasing the (001) and (100)/(010) surface energy and was synthetized solvothermally by Zhao *et al* [111]. A scanning electron microscopy (SEM) image of anatase TiO_2 particle synthesized by microwave-assisted hydrothermal method and its respective Wulff crystal is shown in figure 6.

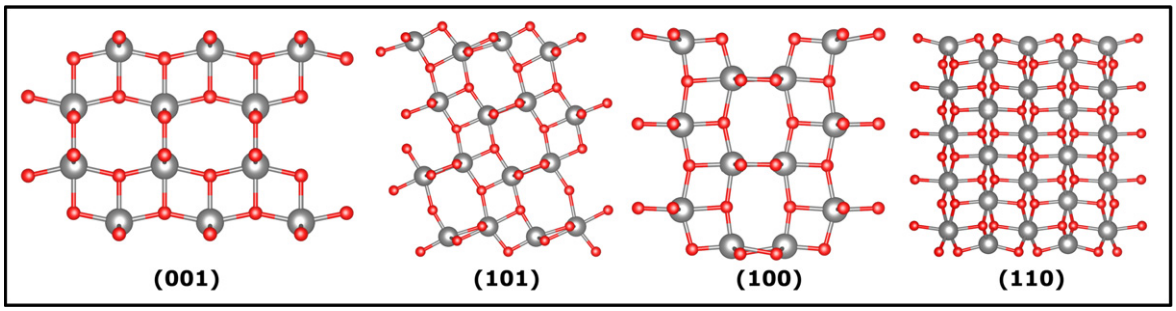

Figure 4. Surface models of (001), (101), (100), and (110) for anatase TiO_2. The red and gray atoms represent O and Ti atoms, respectively.

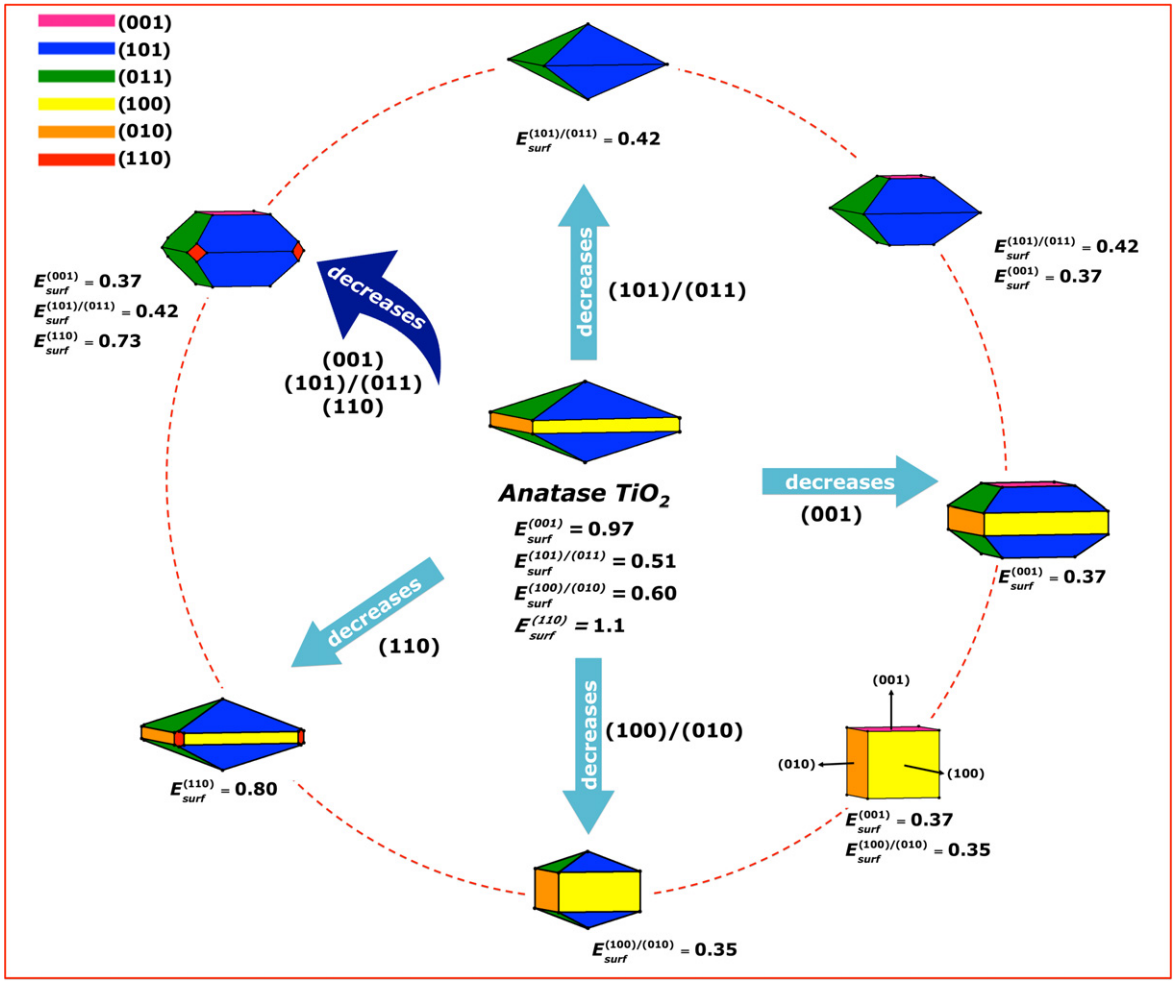

Figure 5. Crystallographic structure and map of morphologies of anatase TiO_2 with crystal planes (001), (101), (011), (100), (010), and (110). Surface energy is in joules per square meter. Theoretical (experimental) [120] lattice parameters, $a = 3.806$ Å (3.78 Å), $c = 9.722$ Å (9.51 Å).

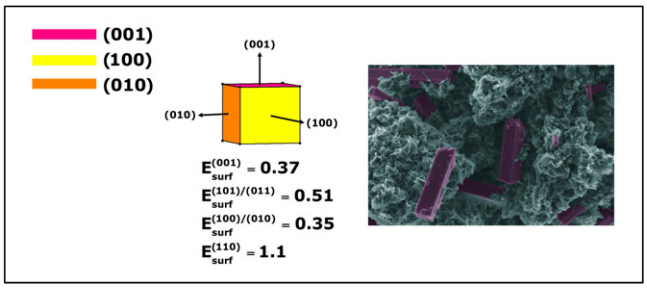

Figure 6. SEM image of cubic anatase TiO_2 particle and its Wulff crystal representation. Surface energy is in joules per square meter.

Even that the TiO_2 particles showed in figure 6 have the same surfaces of the cubic morphology, they present a more elongated shape. This represents lower values of (100)/(010) in relation of (001) surface. According to the Wulff theorem, the larger the difference is, the higher is this elongation.

Decreasing the (101)/(011) and (001) surface energy, we obtained the morphology synthesized by Yang *et al* that shows a breakthrough in synthesizing a truncated tetragonal bipyramid anatase TiO_2 by fluorine capping, resulting in highly exposed (001) facets [42].

The octahedral structure was obtained by Amano *et al* using the hydrothermal reaction to synthetize a morphology with (101) facet [122]. The morphology with (001), (101), and (110) facets, as seen in the map, was obtained by Liu *et al*, which was synthesized using a modified hydrothermal technique in the presence of hydrogen peroxide and hydrofluoric acid solution [123].

3.3. $BaZrO_3$

Barium zirconate ($BaZrO_3$) is a cubic perovskite at normal conditions, exhibiting a unique set of properties such as a high melting point, a small thermal expansion coefficient, small thermal conductivity, and excellent thermal and chemical stability [124]. These properties lead to the use of $BaZrO_3$ in structural applications such as crucibles [125], thermal barrier coatings [126], components in wireless communication systems, the supersonic aircraft industry, and field emission displays, and it is also used as a green photocatalyst [127].

E_{surf} of a plane is highly sensitive to the surface composition, impurities, and distortions/defects of a crystal. When an atom or foreign species becomes adsorbed on one surface or plane, it can decrease/increase the surface energy of that plane and may even stabilize/destabilize it with respect to other planes. Because of this adsorption, anisotropy is created in the surface energies, and this may be responsible for a change in the overall shape of the crystal with the original surface energy plane appearing/disappearing at the surface of the crystal. Traditionally, KOH (as a mineralizer) has often been used to provide an OH^- environment in the hydrothermal crystallization process of ABO_3 perovskite [128]. Morphology changes can also be accomplished by adding impurities/dopants to the system. The dopants act in a different way with respect to the changes in the energy order of the facets, according to the impurity species and their quantity [129].

Calculations for $BaZrO_3$ bulk and surfaces were performed using Monkhorst-Pack special k-points grids ($3 \times 3 \times 1$) to ensure geometrical and energetic convergence for the $BaZrO_3$ structures considered in this work. The (001), (011), and (111) facets are modeled using stoichiometric systems. Slab models containing 6, 8, and 9 molecular units for (001), (011), and (111) surfaces, respectively, were considered, with areas of 18.1 Å^2, 25.5 Å^2, and 31.3 Å^2, respectively. It is worth noting that the stoichiometric (001), (011), and (111) surfaces are BaO and ZrO_2 terminated, O_2 and BaZrO-terminated, and BaO_3 and Zr-terminated, respectively, as illustrated in figure 7.

Figure 8 presents the Wulff´s crystal of the obtained $BaZrO_3$ results. Figure 8 also shows all the possible morphologies that can be obtained by varying the ratio between the E_{surf}, taking into account the (001), (011), and (111) surfaces.

The variation in surface energy using the Wulff construction can be used as a powerful tool to evaluate the morphology of particles because of the difficulty in simulating all the details in a reaction system that interacts with the surface. A SEM image of a $BaZrO_3$ particle synthesized by microwave-assisted hydrothermal method and its respective Wulff crystal is shown in figure 9.

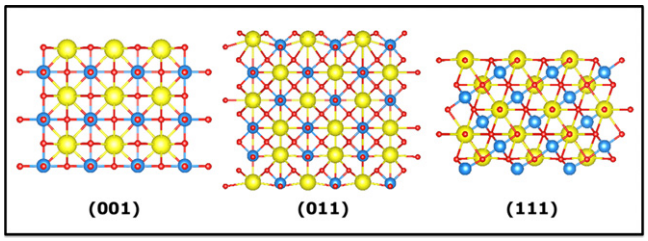

Figure 7. Surface models of (001), (011), and (111) surfaces for $BaZrO_3$. The Ba, Zr, and O atoms are shown in yellow, blue, and red, respectively.

Based on this result, it is possible to determine the relative energy values of each surface in order to obtain the experimental results. Besides the deca-octahedral morphology, Nakashime *et al* [131] reported cubic particles of $BaZrO_3$ synthesized by a composite-hydroxide-mediated approach at low temperature. Moreira *et al* [132] also showed a coexistence of cubic and deca-octahedral $BaZrO_3$ particles obtained by the microwave assisted hydrothermal method. These cases of cubic particles are in agreement with the ideal state (see figure 8).

3.4. α-Ag_2WO_4

Transition metal tungstates are important inorganic materials that are studied and applied widely in many fields [133]. Among these, Ag_2WO_4 has attracted considerable attention because of their potential applications in fields as ionic conductivity [134], photocatalysis [135], sensors [136], microbial agents [137], photoluminescence properties [137, 138].

Ag_2WO_4 has three different crystallographic forms, α-, β-, and γ-Ag_2WO_4, among which α-Ag_2WO_4 is the thermodynamically stable phase that has been investigated [138]. To date, various methods of synthesis such as controlled precipitation [139], hydrothermal [140], and microwave-assisted method [89] have been reported in literature to obtain different Ag_2WO_4 nanostructures.

The (100), (010), (001), (110), (101), and (011) surfaces of α-Ag_2WO_4 were modeled by unreconstructed slab models using a calculated equilibrium geometry and using a ($3 \times 3 \times 1$) Monkhorst-Pack special k-points grid. Slab models containing 8, 8, 16, 10, 9, and 16 molecular units for (100), (010), (001), (110), (101), and (011) surfaces, respectively, were considered, with areas of 68.6 Å^2, 64.1 Å^2, 132.5 Å^2, 93.9 Å^2, 149.2 Å^2, and 147.2 Å^2, respectively. It is worth noting that the (010), (100), (101), and (011) surfaces are O and Ag-terminated, while the (001) and (110) surfaces are O, W, and Ag-terminated. The slab representations are shown in figure 10.

Figure 11 presents the Wulff's crystal of the optimized α-Ag_2WO_4 and the different morphologies that would be obtained assuming different surface energy ratios. An analysis of figure 11 shows that the calculated energy surface values (ideal) generate a prism shape. The ratio of the energy surface

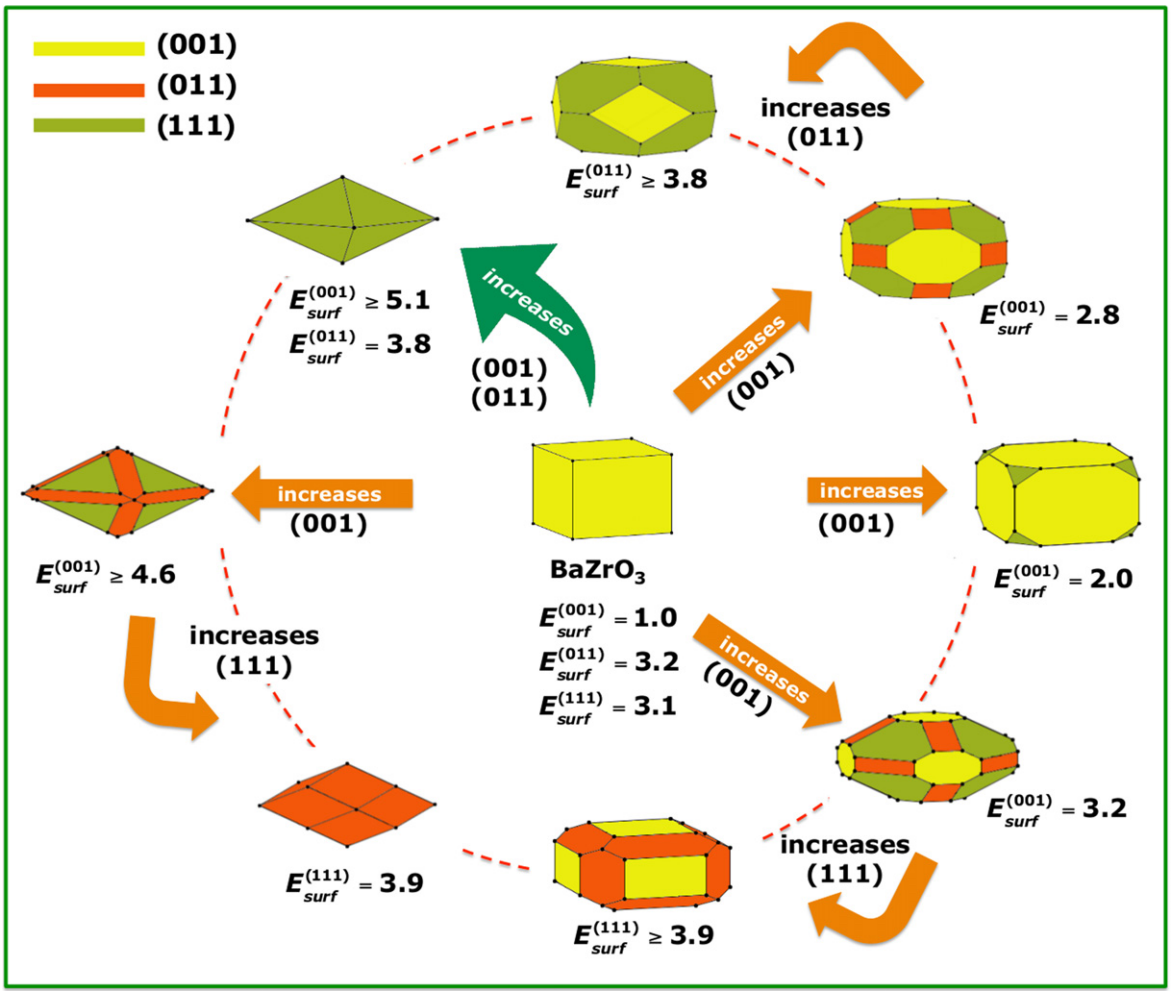

Figure 8. Crystallographic structure and map of morphologies of $BaZrO_3$ with (001), (011), and (111) crystal planes. Surface energy is in joules per square meter. Theoretical (experimental) [130] lattice parameter, $a = 4.251$ Å (4.18 Å).

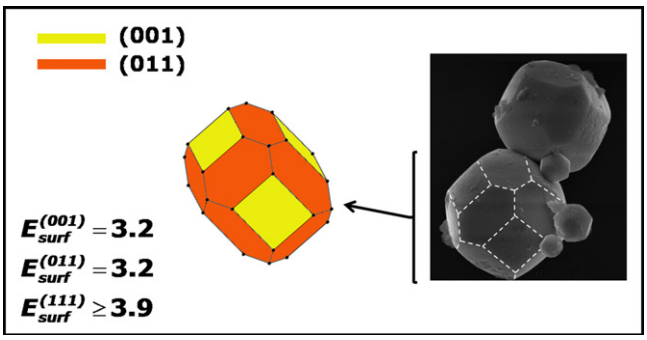

Figure 9. SEM image of deca-octahedral $BaZrO_3$ crystals and its Wulff crystal representation. Surface energy is in joule per·square meter.

has been varied by increasing the value of the more stable surfaces (left in figure 11) and by decreasing the value of the less stable surfaces (right in figure 11).

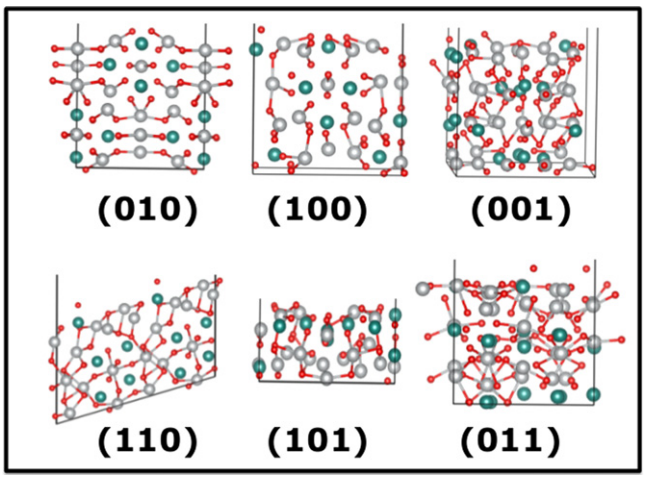

Figure 10. Surface models of (010), (100), (001), (110), (101), and (011) for α-Ag_2WO_4. The Ag, W, and O atoms appear in gray, blue, and red, respectively.

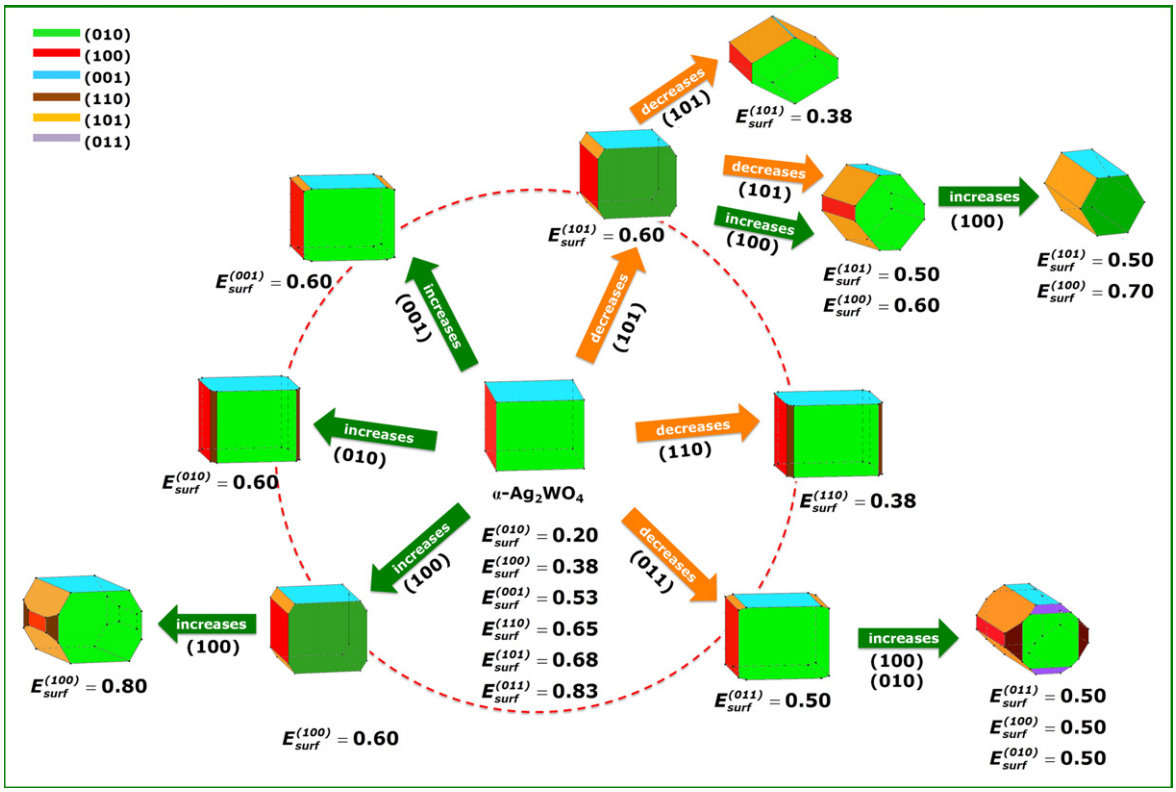

Figure 11. Crystallographic structure and map of morphologies of α-Ag_2WO_4 with crystal planes (010), (100), (001), (110), (101), and (011). Surface energy is in joules per square meter. Theoretical (experimental) [138] lattice parameters, $a = 11.126$ Å (10.87 Å), $b = 11.907$ Å (12.01 Å), $c = 5.761$ Å (5.89 Å).

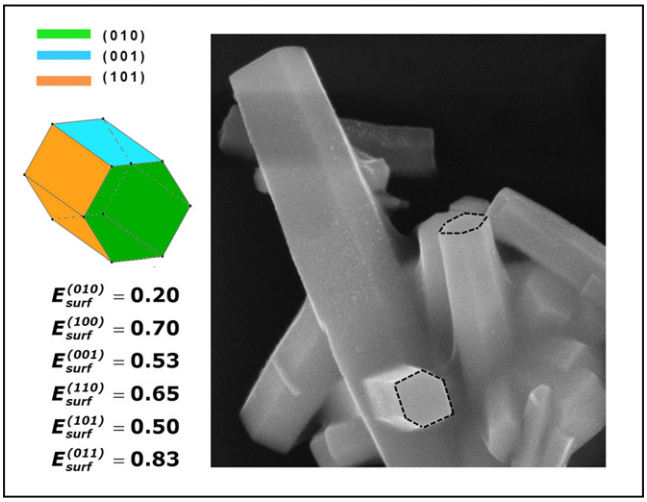

Figure 12. SEM image of α-Ag_2WO_4 crystals and its Wulff crystal representation. Surface energy is in joules per square meter.

A SEM image of α-Ag_2WO_4 particle synthesized by microwave-assisted hydrothermal method and its respective Wulff crystal is shown in figure 12. Besides this image, experimental results reported recently by Roca *et al* [60] show the same hexagonal rod-like shape under certain condition. Assuming the ideal structure as a starting-point, this morphology can be theoretically obtained increasing (101) and (100) surface energys to $0.5\,\mathrm{J\,m^{-2}}$ and $0.7\,\mathrm{J\,m^{-2}}$, respectively.

In summary, the mechanism of the morphology transformation of α-Ag_2WO_4 crystals controlled by surface chemistry has been investigated experimentally and theoretically. The selection of surfaces to investigate was limited to low-index surfaces and surfaces with experimental observations were preferred.

4. Conclusions

The surface is a key component of a solid-state material, as many physical and chemical processes take place on surfaces. A series of materials that includes metal (Ag), simple (anatase TiO_2), and complex ($BaZrO_3$ and α-Ag_2WO_4) metal oxides with fascinating polyhedral morphologies such as octahedral, cuboctahedral, and truncated cubic structures were obtained. A controlled structural transformation between polyhedra is an essential goal of crystal engineering strategies. This framework is envisaged to provide guidelines for the synthesis of crystals of desired morphologies. The main conclusions can be summarized as follows: (i) We successfully demonstrate the morphological modulation of three-dimensional NCs. (ii) Based on the reverse Wulff theorem, we demonstrated that the structural transformations among different morphologies were easily controlled by the relative values of surface energies. (iii) By a proper adjustment of the ratio of the values for the surface energy of different facets, we are

capable of finding a given morphology. This strategy will contribute to a better understanding of the control of morphological characteristics in nano- and micro-crystals. (iv) In the case of Ag and $BaZrO_3$, it was applied a combination of experimental data, obtained from images taken by high-resolution TEM and SEM, respectively, and the calculated surface energies for the three-dimensional Wulff construction. (v) This research will lay the foundations of not only unequivocal shape determination, but also an in-depth understanding of the observed features during the synthesis at the atomic level to help facilitate further breakthroughs in the control of crystal morphology.

Results presented here are an illustration of how first-principles calculations are capable of rationalizing the mechanisms stabilizing the morphology of micro- and nanoparticles at the atomic level. Using the present method, a 3D platform for the morphology modulation of materials with a complete array of accessible morphologies is obtained. We believe that our work has both predictive and explanatory capabilities, and it can be of help in the refinement of both research and technological developments to gain further understanding of how to achieve morphological control of complex three-dimensional crystals from metals to metal oxides.

Acknowledgments

The authors are grateful to FAPESP (2013/07296-2, 2012/14468-1, 2013/26671-9 and 2014/04350-9), CAPES (process A104/2013 and 99999.002998/2014-09), CNPq INCTMN 573636/2008-7, *PrometeoII*/2014/022 and ACOMP/2014/270 projects (Generalitat Valenciana), Ministerio de Economia y Competitividad (Spain), CTQ2012-36253-C03-02 and the Spanish Brazilian program (PHB2009-0065-PC) for financially supporting this research. We also acknowledge the Servei Informática, Universitat Jaume I for a generous allotment of computer time.

References

[1] Kong X Y, Ding Y, Yang R and Wang Z L 2004 *Science* **303** 1348–51
[2] Huang S *et al* 2012 *Dalton Trans.* **41** 5634–42
[3] Wang L and Li Y 2007 *Chem. Mater.* **19** 727–34
[4] Zhai T *et al* 2009 *Adv. Funct. Mater.* **19** 2423–30
[5] Flytzani-Stephanopoulos M and Schmidt L D 1979 *Prog. Surf. Sci.* **9** 83–111
[6] Zhao X *et al* 2008 *Funct. Mater. Lett.* **01** 167–72
[7] Sun C and Xue D 2014 *Cryst. Growth Des.* **14** 2282–7
[8] Chen K, Sun C and Xue D 2015 *Phys. Chem. Chem. Phys.* **17** 732–50
[9] Wulff G 1901 *Z. Kristallogr.* **34** 449–530
[10] Herring C 1951 *Phys. Rev.* **82** 87–93
[11] Roosen A R, McCormack R P and Carter W C 1998 *Comput. Mater. Sci.* **11** 16–26
[12] Zucker R V, Chatain D, Dahmen U, Hagege S and Carter W C 2012 *J. Mater. Sci.* **47** 8290–302
[13] Scopece D 2013 *J. Appl. Crystallogr.* **46** 811–6
[14] Burda C, Chen X, Narayanan R and El-Sayed M A 2005 *Chem. Rev.* **105** 1025–102
[15] Dahl J A, Maddux B L S and Hutchison J E 2007 *Chem. Rev.* **107** 2228–69
[16] Lu A-H, Salabas E L and Schüth F 2007 *Angew. Chem., Int. Ed.* **46** 1222–44
[17] Murray C B, Kagan C R and Bawendi M G 2000 *Annu. Rev. Mater. Sci.* **30** 545–610
[18] Sun S, Murray C B, Weller D, Folks L and Moser A 2000 *Science* **287** 1989–92
[19] Xia Y, Xiong Y, Lim B and Skrabalak S E 2009 *Angew. Chem., Int. Ed.* **48** 60–103
[20] Kang Y, Pyo J B, Ye X, Gordon T R and Murray C B 2012 *ACS Nano* **6** 5642–7
[21] Kang Y *et al* 2012 *ACS Nano* **7** 645–53
[22] Peng X *et al* 2000 *Nature* **404** 59–61
[23] Ye X *et al* 2010 *Proc. Natl Acad. Sci. USA* **107** 22430–5
[24] Song Q, Ding Y, Wang Z L and Zhang Z J 2006 *J. Phys. Chem.* B **110** 25547–50
[25] Somorjai G A 1981 *Chemistry in Two Dimensions: Surfaces* (Ithaca, NY: Cornell University Press)
[26] Zangwill A 1988 *Physics at Surfaces* (Cambridge: Cambridge University Press)
[27] Wang Z L 2000 *J. Phys. Chem.* B **104** 1153–75
[28] Zhang G *et al* 2010 *Appl. Surf. Sci.* **257** 302–5
[29] Di W, Willinger M-G, Ferreira R A S, Ren X, Lu S and Pinna N 2008 *J. Phys. Chem.* C **112** 18815–20
[30] Yajuan S *et al* 2007 *Nanotechnology* **18** 275609
[31] Xia Y, Xiong Y, Lim B and Skrabalak S E 2009 *Angew. Chem.* **121** 62–108
[32] Wen H *et al* 2008 *J. Phys. Chem.* C **112** 15948–55
[33] Li Z, Lai X, Wang H, Mao D, Xing C and Wang D 2009 *Nanotechnology* **20** 245603
[34] Jian J K *et al* 2007 *J. Cryst. Growth* **303** 427–32
[35] Wang H *et al* 2010 *J. Am. Chem. Soc.* **132** 15875–7
[36] Bratlie K M, Lee H, Komvopoulos K, Yang P and Somorjai G A 2007 *Nano Lett.* **7** 3097–101
[37] Narayanan R and El-Sayed M A 2004 *Nano Lett.* **4** 1343–8
[38] Ferrando R, Jellinek J and Johnston R L 2008 *Chem. Rev.* **108** 845–910
[39] Buhro W E and Colvin V L 2003 *Nat. Mater.* **2** 138–9
[40] Lim B *et al* 2009 *Science* **324** 1302–5
[41] Xie X, Li Y, Liu Z-Q, Haruta M and Shen W 2009 *Nature* **458** 746–9
[42] Yang H G *et al* 2008 *Nature* **453** 638–41
[43] Joo J, Chow B Y, Prakash M, Boyden E S and Jacobson J M 2011 *Nat. Mater.* **10** 596–601
[44] Jiang H B *et al* 2011 *Angew. Chem., Int. Ed.* **50** 3764–8
[45] Dong J J *et al* 2011 *ACS Appl. Mater. Interfaces* **3** 4388–95
[46] Kiatkittipong K, Scott J and Amal R 2011 *ACS Appl. Mater. Interfaces* **3** 3988–96
[47] Maiyalagan T, Chemelewski K R and Manthiram A 2013 *ACS Catal.* **4** 421–5
[48] Duan J, Chen S, Dai S and Qiao S Z 2014 *Adv. Funct. Mater.* **24** 2072–8
[49] Yang W *et al* 2013 *Electrochem. Commun.* **28** 13–6
[50] De Angelis F, Di Valentin C, Fantacci S, Vittadini A and Selloni A 2014 *Chem. Rev.* **114** 9708–53
[51] Mudunkotuwa I A and Grassian V H 2011 *J. Environ. Monit.* **13** 1135–44
[52] Karim A, Fosse S and Persson K A 2013 *Phys. Rev.* B **87** 075322
[53] Kanaki E, Gohr S, Mueller C and Paulus B 2015 *Surf. Sci.* **632** 158–63
[54] Barmparis G D, Lodziana Z, Lopez N and Remediakis I N 2015 *Beilstein J. Nanotechnol.* **6** 361–8
[55] Beltrán A, Andrés J, Longo E and Leite E R 2003 *Appl. Phys. Lett.* **83** 635–7

[56] Leite E R, Giraldi T R, Pontes F M, Longo E, Beltrán A and Andrés J 2003 *Appl. Phys. Lett.* **83** 1566–8
[57] Stroppa D G *et al* 2014 *Phys. Chem. Chem. Phys.* **16** 1089–94
[58] Bomio M R D *et al* 2013 *J. Phys. Chem.* C **117** 21382–95
[59] Longo V M *et al* 2011 *J. Phys. Chem.* C **115** 20113–9
[60] Roca R A *et al* 2015 *Catal. Sci. Technol.* **5** 4091–107
[61] Roca R A and Leite E R 2013 *J. Am. Ceram. Soc.* **96** 96–102
[62] Kresse G and Furthmuller J 1996 *Comput. Mater. Sci.* **6** 15–50
[63] Kresse G and Hafner J 1994 *Phys. Rev.* B **49** 14251–69
[64] Perdew J P, Burke K and Ernzerhof M 1996 *Phys. Rev. Lett.* **77** 3865–8
[65] Kresse G and Joubert D 1999 *Phys. Rev.* B **59** 1758–75
[66] Heid R, Pintschovius L, Reichardt W and Bohnen K P 2000 *Phys. Rev.* B **61** 12059–62
[67] McBride J R, Hass K C and Weber W H 1991 *Phys. Rev.* B **44** 5016–28
[68] Baetzold R C and Yang H 2003 *J. Phys. Chem.* B **107** 14357–64
[69] Barnard A S and Zapol P 2004 *J. Chem. Phys.* **121** 4276–83
[70] Chizallet C *et al* 2008 *J. Phys. Chem.* C **112** 16629–37
[71] Zasada F *et al* 2011 *J. Phys. Chem.* C **115** 6423–32
[72] Vittadini A, Casarin M and Selloni A 2009 *J. Phys. Chem.* C **113** 18973–7
[73] Rogal J, Reuter K and Scheffler M 2004 *Phys. Rev.* B **69** 075421
[74] Lodziana Z, Topsoe N-Y and Norskov J K 2004 *Nat. Mater.* **3** 289–93
[75] Selçuk S and Selloni A 2013 *J. Phys. Chem.* C **117** 6358–62
[76] Wang Y *et al* 2014 *Phys. Rev.* B **90** 045304
[77] Rusanov A I 2005 *Surf. Sci. Rep.* **58** 111–239
[78] Seyed-Razavi A, Snook I K and Barnard A S 2010 *J. Mater. Chem.* **20** 416–21
[79] Jiang Z-Y, Kuang Q, Xie Z-X and Zheng L-S 2010 *Adv. Funct. Mater.* **20** 3634–45
[80] Lee K, Kim M and Kim H 2010 *J. Mater. Chem.* **20** 3791–8
[81] Chernov A A 1963 *Sov. Phys. Crystallogr.* **7** 728–30
[82] Sun Q, Yerino C D, Leung B, Han J and Coltrin M E 2011 *J. Appl. Phys.* **110** 053517
[83] Romanyuk K, Cherepanov V and Voigtländer B 2007 *Phys. Rev. Lett.* **99** 126103
[84] Gross E, LiuJack H-C, Toste F D and Somorjai G A 2012 *Nat. Chem.* **4** 947–52
[85] Heveling J 2012 *J. Chem. Educ.* **89** 1530–6
[86] Rycenga M *et al* 2011 *Chem. Rev.* **111** 3669–712
[87] Zhang J, Li S, Wu J, Schatz G C and Mirkin C A 2009 *Angew. Chem., Int. Ed.* **48** 7787–91
[88] Xia X, Zeng J, Zhang Q, Moran C H and Xia Y 2012 *J. Phys. Chem.* C **116** 21647–56
[89] Longo E *et al* 2013 *Sci. Rep.* **3** 1676
[90] Andrés J *et al* 2014 *Sci. Rep.* **4** 5391
[91] Woehl T J, Park C, Evans J E, Arslan I, Ristenpart W D and Browning N D 2013 *Nano Lett.* **14** 373–8
[92] Li D, Nielsen M H, Lee J R I, Frandsen C, Banfield J F and De Yoreo J J 2012 *Science* **336** 1014–8
[93] Batson P E, Reyes-Coronado A, Barrera R G, Rivacoba A, Echenique P M and Aizpurua J 2011 *Nano Lett.* **11** 3388–93
[94] Elechiguerra J L, Reyes-Gasga J and Yacaman M J 2006 *J. Mater. Chem.* **16** 3906–19
[95] Rashkeev S N, Lupini A R, Overbury S H, Pennycook S J and Pantelides S T 2007 *Phys. Rev.* B **76** 035438
[96] Arumugam S K, Sastry T P, Sreedhar B and Mandal A B 2007 *J. Biomed. Mater. Res.* A **80A** 391–8
[97] Yu A K, Kudrinskiy A A, Olenin A Y and Lisichkin G V 2008 *Russ. Chem. Rev.* **77** 233
[98] González A L, Noguez C, Beránek J and Barnard A S 2014 *J. Phys. Chem.* C **118** 9128–36
[99] Sau T K and Rogach A L 2012 *Complex-Shaped Metal Nanoparticles: Bottom-Up Syntheses and Applications* (Weinheim: Wiley)
[100] Barnard A S 2014 *Nanoscale* **6** 9983–90
[101] Wang Y, He J, Liu C, Chong W H and Chen H 2014 *Angew. Chem., Int. Ed.* **53** 2–32
[102] Spreadborough J and Christian J W 1959 *J. Sci. Instrum.* **36** 116–8
[103] Chen D and Caruso R A 2013 *Adv. Funct. Mater.* **23** 1356–74
[104] Liu L and Chen X 2014 *Chem. Rev.* **114** 9890–918
[105] Bourikas K, Kordulis C and Lycourghiotis A 2014 *Chem. Rev.* **114** 9754–823
[106] Diebold U 2003 *Surf. Sci. Rep.* **48** 53–229
[107] Barnard A S and Curtiss L A 2005 *Nano Lett.* **5** 1261–6
[108] Yang H G and Zeng H C 2004 *J. Phys. Chem.* B **108** 3492–5
[109] Gong X-Q and Selloni A 2005 *J. Phys. Chem.* B **109** 19560–2
[110] Wen C Z, Zhou J Z, Jiang H B, Hu Q H, Qiao S Z and Yang H G 2011 *Chem. Commun.* **47** 4400–2
[111] Zhao X *et al* 2011 *Adv. Funct. Mater.* **21** 3554–63
[112] Wang Y, Zhang H, Han Y, Liu P, Yao X and Zhao H 2011 *Chem. Commun.* **47** 2829–31
[113] Dinh C-T, Nguyen T-D, Kleitz F and Do T-O 2009 *ACS Nano* **3** 3737–43
[114] Wen C Z, Hu Q H, Guo Y N, Gong X Q, Qiao S Z and Yang H G 2011 *Chem. Commun.* **47** 6138–40
[115] Xiang Q, Yu J, Wang W and Jaroniec M 2011 *Chem. Commun.* **47** 6906–8
[116] Pan J, Liu G, Lu G Q and Cheng H-M 2011 *Angew. Chem., Int. Ed.* **50** 2133–7
[117] D'Arienzo M *et al* 2011 *J. Am. Chem. Soc.* **133** 17652–61
[118] Tachikawa T, Yamashita S and Majima T 2011 *J. Am. Chem. Soc.* **133** 7197–204
[119] Bandura A V, Evarestov R A and Kuruch D D 2010 *Surf. Sci.* **604** 1591–7
[120] Moura K F *et al* 2014 *J. Solid State Chem.* **210** 171–7
[121] Barnard A S, Zapol P and Curtiss L A 2005 *J. Chem. Theory Comput.* **1** 107–16
[122] Amano F, Yasumoto T, Prieto-Mahaney O-O, Uchida S, Shibayama T and Ohtani B 2009 *Chem. Commun.* **17** 2311–3
[123] Liu M *et al* 2010 *Chem. Commun.* **46** 1664–6
[124] Kumar H P *et al* 2008 *J. Alloys Compd.* **458** 528–31
[125] Dierickx D, Houben I, Lapin J, Delannay F and Van Der Biest O 1996 *J. Mater. Sci. Lett.* **15** 1573–6
[126] Pan L, Li L and Chen Y 2013 *J. Sol-Gel Sci. Technol.* **66** 330–6
[127] Yuan Y *et al* 2008 *Int. J. Hydrogen Energy* **33** 5941–6
[128] Wang D *et al* 2002 *Solid State Ion.* **151** 329–33
[129] Alfredsson M *et al* 2007 *Surf. Sci.* **601** 4793–800
[130] Moreira M L, Andres J, Varela J A and Longo E 2009 *Cryst. Growth Des.* **9** 833–9
[131] Nakashima K, Fujii I and Wada S 2011 *J. Ceram. Soc. Japan* **119** 532–4
[132] Moreira M L *et al* 2011 *Scr. Mater.* **64** 118–21
[133] Yu S H, Liu B, Mo M S, Huang J H, Liu X M and Qian Y T 2003 *Adv. Funct. Mater.* **13** 639–47
[134] Suthanthiraraj S A and Sarojini S 2012 *Chem. Sci. Trans.* **1** 13–22
[135] Tang J and Ye J 2005 *J. Mater. Chem.* **15** 4246–51
[136] da Silva L F *et al* 2014 *Nanoscale* **6** 4058–62
[137] Longo V M *et al* 2014 *J. Phys. Chem.* A **118** 5769–78
[138] Cavalcante L S *et al* 2012 *Inorg. Chem.* **51** 10675–87
[139] Wang X, Li S, Yu H and Yu J 2011 *J. Mol. Catal.* A **334** 52–9
[140] Liu X *et al* 2013 *Mater. Lett.* **91** 129–32